

Chapter 2

Early Universe Cosmology

The main intention of this thesis is to motivate and investigate the B – L phase transition as the possible origin for the thermal phase of the hot early universe. Before we are ready to do so, we have to acquaint ourselves with the observational evidence for this phase and understand which physical processes have or may have taken place in it. For this reason we shall provide a brief review of early universe cosmology in this chapter, thereby compiling the background material for the further discussion. We will first discuss the present composition of the universe (cf. Sect. 2.1) and then some of the main events in the thermal history of the universe in reverse chronological order (cf. Sect. 2.2). We would like to emphasize that in this introductory chapter we will crudely restrict ourselves to aspects which are relevant for our purposes. More balanced and comprehensive presentations of the topic are for instance provided in standard textbooks [1–3] or dedicated review articles [4–6].

2.1 Composition of the Universe

Over the last years the observational progress has marked the advent of the era of precision cosmology. The combined data exhibits an impressive consistency and is in very good agreement with the currently accepted concordance model of big bang cosmology, the Lambda-Cold Dark Matter (Λ CDM) model. Major evidence for this standard scenario of big bang cosmology derives from several cosmological observations, the most eminent being perhaps (i) the observed primordial abundances of the light elements, matching very well the theoretical prediction from BBN [6], (ii) the angular power spectrum of the temperature anisotropies in the CMB as measured by the Wilkinson Microwave Anisotropy Probe (WMAP) satellite [7], (iii) the imprint of baryonic acoustic oscillations (BAOs) in the local distribution of matter as seen in galaxy surveys [8], (iv) direct measurements of the cosmic expansion rate, i.e. the Hubble parameter H_0 , by the Hubble Space Telescope [9], and (v) distance measurements based on type Ia supernovae (SNe) [10, 11].

All observed cosmological phenomena are consistent with the assumption that our universe is spatially flat [7, 12]. Indeed, combining the data on CMB anisotropies, BAOs and H_0 shows that presently, at 95 % CL, the total energy density of the universe ρ_{tot} does not deviate by more than 1 % from the critical energy density ρ_c that is required for exact spatial flatness. In the following we shall hence neglect the possibility of a small spatial curvature and assume that $\rho_{\text{tot}} = \rho_c$, which is equivalent to saying that all density parameters Ω_i sum to unity,

$$\Omega_{\text{tot}} = \sum_i \Omega_i = \sum_i \frac{\rho_i}{\rho_c} = \frac{\rho_{\text{tot}}}{\rho_c} = 1. \quad (2.1)$$

This sum receives contributions from three different forms of energy or matter: radiation, matter and dark energy. In the present epoch the energy in radiation from beyond our galaxy is dominated by the photons of the CMB. Relic neutrinos which are presumed to be present in the current universe as a remnant of the hot early universe either belong to radiation or matter, depending on their absolute masses. The matter component splits into a small baryonic and a large dark nonbaryonic fraction. We shall now discuss in turn how photons, neutrinos, baryonic matter, dark matter and dark energy respectively contribute to Ω_{tot} .

2.1.1 CMB Photons

In the early 1990's the Cosmic Background Explorer (COBE) satellite experiment was the first precision measurement to confirm two key features of the CMB. Since COBE we know that the CMB has an almost perfect Planckian spectrum [13, 14] and that it is highly isotropic, with its temperature fluctuating across the sky only at the level of 10^{-5} [15]. Together, these findings provide strong evidence for a hot thermal phase in the early universe preceded by an inflationary era (cf. Sect. 2.2.1). The mean CMB temperature is $T_\gamma^0 = 2.7255(6)$ K [16]. Given the thermal black-body distribution of the CMB photons, this temperature directly implies the following entropy, number and energy densities

$$s_\gamma^0 \simeq 1,500 \text{ cm}^{-3}, \quad n_\gamma^0 \simeq 410 \text{ cm}^{-3}, \quad \rho_\gamma^0 \simeq 260 \text{ meV cm}^{-3}. \quad (2.2)$$

The present value of the critical energy density is determined by the current expansion rate. With the aid of the dimensionless Hubble parameter h , which is defined through the relation $H_0 = 100 h \text{ km/s/Mpc}$, we are able to write ρ_c^0 as

$$\rho_c^0 = \frac{3M_P^2}{8\pi} H_0^2 \simeq 10.54 h^2 \text{ keV cm}^{-3}, \quad (2.3)$$

with $M_P \simeq 1.22 \times 10^{19} \text{ GeV}$ denoting the Planck mass. The Λ CDM fit to the combined CMB, BAO and H_0 data gives $h \simeq 0.704$ [7], such that $\rho_c^0 \simeq 5,200 \text{ eV cm}^{-3}$,

which results in a photon density parameter

$$\Omega_\gamma^0 \simeq 5 \times 10^{-5}. \quad (2.4)$$

Barring some unknown form of dark radiation [17], the only other significant contribution to the present-day entropy density in radiation comes from neutrinos.¹ We thus conclude that photons are responsible for a large fraction of the radiation entropy in the current universe, but contribute only to a negligible extent to the total energy density.

2.1.2 Relic Neutrinos

In the hot early universe neutrinos are produced and kept in thermal equilibrium via weak interactions. Around a temperature $T \sim 1$ MeV the rate of these interactions drops below the Hubble rate, causing the neutrinos to decouple from the thermal bath and evolve independently of all other species afterwards. The presence of a relic abundance of primordial neutrinos in the current universe is hence a fundamental prediction of the hot big bang scenario. It is doubtful whether this cosmic neutrino background (CNB) will ever be directly observed, as the low-energetic CNB neutrinos interact only extremely weakly [19]. By contrast, a series of physical processes in the early universe such as BBN, the evolution of the CMB temperature anisotropies or the formation of matter structures on large scales are fortunately sensitive to the influence of primordial neutrinos, which provides us with compelling indirect evidence for their existence [20, 21].

The observed oscillations between the three neutrino flavours [22, 23] indicate that neutrinos have small masses.² This has a direct impact on their evolution after decoupling. If neutrinos were massless, their temperature T_ν would decrease for the most part in parallel to the photon temperature T_γ as the universe continues to expand. Only at photon temperatures around the electron mass $m_e \simeq 511$ keV, T_γ and T_ν would behave slightly differently. Around $T_\gamma \sim m_e$, the thermal production of electrons and positrons begins to cease. e^+e^- annihilations into photons then deposit the entire energy formerly contained in electrons and positrons in the photon component, which slows down the decline of T_γ for a short time, but not the decline of T_ν . For massless neutrinos entropy conservation would imply $T_\nu^0 = (4/11)^{1/3} T_\gamma^0 \simeq 1.9$ K and neutrinos would presently have a density $\Omega_\nu^0 \simeq 3 \times 10^{-5}$. The energy density of massive neutrinos, however, experiences a slower redshift due to the cosmic expansion than the energy density of massless neutrinos. While the energy of a massless

¹ Note that in the recent cosmic past, shortly after the onset of star formation, the entropy contained in black holes has come to dominate over the entropy in radiation [18].

² In the following discussion we shall restrict ourselves to the relic abundance of primordial neutrinos. If neutrinos are Dirac fermions, the abundance of antineutrinos should at each time be approximately the same as the abundance of neutrinos.

neutrino goes to zero as the universe expands, the energy E_{ν_i} of a neutrino mass eigenstate with mass $m_{\nu_i} \neq 0$ asymptotically approaches m_{ν_i} . Once the energy of a massive neutrino is dominated by its mass rather than its momentum, it becomes nonrelativistic. For sufficiently large neutrino masses, the energy contained in nonrelativistic neutrinos thus outweighs by far the energy of neutrinos that are still relativistic, such that the present neutrino density is well described by

$$\Omega_\nu^0 h^2 \simeq \frac{m_{\nu,\text{tot}}}{94 \text{ eV}}, \quad m_{\nu,\text{tot}} = \sum_{\nu_i} m_{\nu_i}, \quad (2.5)$$

where the sum runs over all mass eigenstates that have turned nonrelativistic at some value of T_γ below 1 MeV, i.e., given the measured mass squared differences, over at least two out of three states. The lower bound on the sum of neutrino masses implied by the mass squared differences is roughly 0.05 eV, so that $\Omega_\nu^0 \gtrsim 1 \times 10^{-3}$. On the other hand, several cosmological observations constrain $m_{\nu,\text{tot}}$ from above. Massive free-streaming neutrinos damp the growth of matter fluctuations and could thus leave an imprint in large-scale structure (LSS) observables [24, 25]. So far, no effects from neutrino masses have yet been observed. Instead, combining data from galaxy surveys, WMAP, BAO, H_0 and type Ia SNe, one is able to put an upper limit of 0.28 eV on $m_{\nu,\text{tot}}$ [26], which corresponds to $\Omega_\nu^0 \lesssim 6 \times 10^{-3}$.

After leaving thermal equilibrium, most neutrinos never again interact with other particles. The entropy and total number of neutrinos hence remain practically unchanged after decoupling, which is why we speak of the neutrinos as being *frozen out*. At the time neutrinos decouple, they are relativistic. Their entropy and number densities thus subsequently always evolve as the corresponding densities of massless neutrinos would do, independently of the fact that neutrinos are actually massive, turning nonrelativistic at lower temperatures. Because of this peculiar thermal history, neutrinos represent a prime example for what is often referred to as *hot relics*. With the aid of the would-be temperature of massless neutrinos, $T_\nu^0 \simeq 1.9 \text{ K}$, we then obtain $s_\nu^0 \simeq 1,400 \text{ cm}^{-3}$ and $n_\nu^0 \simeq 340 \text{ cm}^{-3}$.

In conclusion, we find that also neutrinos contribute only to a negligibly small extent to the total energy density of the universe,

$$1 \times 10^{-3} \lesssim \Omega_\nu^0 \lesssim 6 \times 10^{-3}, \quad (2.6)$$

which follows from Eq. (2.5) and the bounds on the total neutrino mass,

$$0.05 \text{ eV} \lesssim m_{\nu,\text{tot}} \lesssim 0.28 \text{ eV}. \quad (2.7)$$

In return, their entropy density is almost as large as the one of the CMB photons. The present radiation entropy density s_R^0 , comprising the photon entropy density and the entropy densities of all hot relics, i.e. neutrinos in the standard hot big bang scenario, then turns out to be

$$s_R^0 = s_\gamma^0 + s_\nu^0 \simeq 2,900 \text{ cm}^{-3}. \quad (2.8)$$

Note that, by definition, s_R^0 can also be written as the entropy of a thermal bath with an effective number of degrees of freedom $g_{*,s}^0$ at temperature T_γ^0 ,

$$s_R^0 = \frac{2\pi^2}{45} g_{*,s}^0 (T_\gamma^0)^3, \quad g_{*,s}^0 = 2 + \frac{7}{8} \cdot 3 \cdot 2 \cdot \frac{4}{11} = \frac{43}{11}. \quad (2.9)$$

The entropy associated with this density directly corresponds to the entropy inherent in the thermal bath during the hot phase of the early universe. A conclusive explanation for its origin is still lacking and it is a major task of modern particle cosmology to explore possible sources for this primordial entropy. A key motivation of this thesis is to demonstrate that the spontaneous breaking of $B-L$ at the end of inflation represents a viable scenario for its generation.

2.1.3 Baryonic Matter

All forms of matter in the universe that can be more or less well described by standard particle physics, such as gas clouds, stars, planets, black holes, etc., are baryonic, i.e. made out of ordinary atoms, whose nuclei are composed of protons and neutrons.³ The present abundance of these baryons, or more precisely nucleons, is conveniently parametrized in terms of the baryon-to-photon ratio η_b ,

$$\Omega_b^0 h^2 = \frac{m_N}{\rho_c^0 / h^2} n_\gamma^0 \eta_b^0 \simeq \frac{1}{273} \left(\frac{\eta_b^0}{10^{-10}} \right), \quad \eta_b^0 = \frac{n_b^0}{n_\gamma^0}. \quad (2.10)$$

where $m_N \simeq 940 \text{ MeV}$ is the mass of a single nucleon, n_b^0 denotes the present number density of baryons, and where we have used the value for n_γ^0 stated in Eq. (2.2). In the standard BBN scenario with three generations of relativistic neutrinos, the primordial abundances of the light nuclei are solely controlled by the baryon-to-photon ratio (cf. Sect. 2.2.2). The measurement of these abundances hence provides us with an observational handle on η_b^0 . Matching the observed abundances with the theoretical BBN prediction, one finds at 95 % CL [6]

$$\text{BBN:} \quad 5.1 \times 10^{-10} \leq \eta_b^0 \leq 6.5 \times 10^{-10}, \quad 0.019 \leq \Omega_b^0 h^2 \leq 0.024. \quad (2.11)$$

One of the key predictions of standard cosmology is that between BBN and the decoupling of the CMB the number of baryons as well as the photon entropy are

³ In order to ensure that the universe as a whole is electrically charge neutral, there has to be present one electron for each proton in the universe. As a single proton is, however, roughly 1,800 times heavier than an electron, the contribution from electrons to the total energy presently stored in matter is negligibly small, which is why we will not consider it any further.

conserved such that the baryon-to-photon ratio remains unchanged between these two processes. This prediction can be observationally tested as the CMB power spectrum is fortunately very sensitive to the physical baryon density $\rho_b \propto \Omega_b h^2$ (cf. Sect. 2.2.1). Fitting the Λ CDM model to the CMB data yields [7]

$$\text{CMB: } \eta_b^0 \simeq (6.18 \pm 0.14) \times 10^{-10}, \quad \Omega_b^0 h^2 = 0.02260 \pm 0.00053, \quad (2.12)$$

which is consistent with the BBN result in Eq. (2.11) and hence serves as yet another endorsement of the standard picture. The agreement between the two determinations of η_b^0 is particularly remarkable in so far as they probe completely different physical processes occurring in two widely separated epochs. Due to its high precision, we will from now on, after some additional rounding, use the CMB value as our estimate for the present baryon-to-photon ratio, $\eta_b^{\text{obs}} = 6.2 \times 10^{-10}$, which corresponds to a baryon density parameter $\Omega_b^0 \simeq 4.6 \times 10^{-2}$.

Depending on the perspective, we are led to the conclusion that the present abundance of baryons in the universe is either exceptionally low or high. First of all, it is surprising that BBN and the CMB concordantly imply that only a fraction of roughly 5 % of the total energy of the universe resides in baryons. In view of the fact that our universe appears to be spatially flat, one might rather expect a baryon density parameter $\Omega_b^0 \simeq 1$. The low abundance of baryons is hence an indication for the presence of other nonbaryonic forms of matter or energy, viz. dark matter and dark energy, that account for 95 % of the energy budget of the universe. On the other hand Ω_b^0 is remarkably large compared to the theoretical expectation.⁴ In the early universe the baryon-to-photon ratio freezes out when the baryons decouple from the thermal bath at temperatures of $\mathcal{O}(10..100)$ MeV. Assuming that the universe is locally baryon-antibaryon symmetric down to temperatures of this magnitude, the annihilation of baryon-antibaryon pairs shortly before decoupling would dramatically reduce the abundances of both baryons and antibaryons. In consequence of this *annihilation catastrophe* the present baryon-to-photon would be nine orders of magnitude smaller than the observed value, $\eta_b^0 \simeq 5 \times 10^{-19}$ [1, 29]. The most reasonable way out of the annihilation catastrophe is the possibility that the universe possesses a baryon-antibaryon asymmetry at temperatures of $\mathcal{O}(100)$ MeV. The excess of baryons over antibaryons at the time of annihilation would then explain the large observed baryon abundance.

Further evidence for a primordial baryon asymmetry comes from the fact that the observable universe seems to contain almost exclusively matter and almost no antimatter.⁵ If there were to exist large areas of antimatter in the universe, annihilation processes along the boundaries between the matter and antimatter domains would

⁴ It is also large compared to the observed abundance of luminous matter. The density parameter of stars is smaller than Ω_b^0 by one order of magnitude, $\Omega_{\text{stars}} \simeq 2.7 \times 10^{-3}$ [27]. Most baryons are thus optically dark, probably contained in some diffuse intergalactic medium [28].

⁵ Antiparticles of cosmic origin such as antiprotons and positrons are seen in cosmic rays. Their fluxes are, however, consistent with the assumption that they are merely secondaries produced in energetic collisions of cosmic rays with the interstellar medium rather than primordial relics.

result in characteristic gamma ray signals. As no such signals have yet been observed, the local abundance of antimatter can be tightly constrained on a multitude of length scales, ranging from our solar system, to galaxies and clusters of galaxies. X- and gamma-ray observations of the Bullet Cluster, a system of two colliding galaxy clusters, put for instance an upper bound of 3×10^{-6} on the local antimatter fraction, thus ruling out serious amounts of antimatter on scales of $\mathcal{O}(20)$ Mpc, which are the largest scales directly probed so far [30]. Furthermore, assuming that matter and antimatter are present in equal shares on cosmological scales, one can show that the matter domain we inhabit virtually has to cover the entire visible universe [31].

The absence of antimatter in our universe thus allows for a different interpretation of the baryon-to-photon ratio η_b^0 . As the ratio of photons to antibaryons is practically zero, η_b^0 can also be regarded as a measure for the baryon asymmetry of the universe (BAU),

$$\eta_b^0 = \frac{n_b^0}{n_\gamma^0} \rightarrow \frac{n_b^0 - n_{\bar{b}}^0}{n_\gamma^0}. \quad (2.13)$$

To emphasize this different interpretation of the baryon-to-photon ratio we will write η_B^0 instead of η_b^0 in the following, where the subscript B is supposed to refer to the total baryon number of the universe. Again, standard cosmology lacks an explanation for the origin of this primordial asymmetry. A second key motivation for this thesis is hence to identify a natural mechanism for the dynamical generation of the BAU that can be consistently embedded into an overall picture of the early universe. As we will demonstrate, leptogenesis after nonthermal neutrino production in the decay of B - L Higgs bosons represents a viable and particularly attractive option.

2.1.4 Dark Matter

A plethora of astrophysical and cosmological observations indicates that next to ordinary matter some form of dark matter (DM), i.e. nonluminous and nonabsorbing matter which reveals its existence only through its gravitational influence on visible matter, is ubiquitously present in the universe.⁶ Direct evidence for dark matter derives from all observable length scales. The rotation curves of spiral galaxies as well as the velocity dispersions of stars in elliptical galaxies probe the abundance of dark matter on the scale of individual galaxies.⁷ This applies in particular to our

⁶ For recent reviews on dark matter, cf. for instance Refs. [32–35]. Another ansatz to account for the various observed, but unexplained gravitational effects is to modify the theory of general relativity. While modifications of gravity (cf. in particular Refs. [36, 37]) are often able to explain isolated phenomena, they usually struggle to give a consistent description of all observed phenomena, which is why we will not consider them any further in this thesis.

⁷ Seminal works in this field have been the observations by Vera Rubin and Kent Ford, who measured the rotation curve of the Andromeda Nebula in 1970 [38], as well as by Sandra Faber and Robert Jackson, who studied stellar velocities in elliptical galaxies in 1976 [39].

own galaxy, whose rotation curve in combination with other data allows to determine the fraction of dark matter in the neighborhood of our solar system quite precisely [40]. On the scale of clusters of galaxies, peculiar galaxy velocities in virialized galaxy clusters, X-ray observations of the hot intracluster gas and gravitational lensing effects on background galaxies point to large amounts of dark matter.⁸ Especially compelling evidence for dark matter comes from detailed studies of the Bullet Cluster, whose dynamics can only be understood if it is assumed to be predominantly composed of very weakly self-interacting dark matter [42]. Finally, on cosmological scales the presence of dark matter is implied by the theory of structure formation. If the presently observed LSS of matter in the universe was to be traced back only to the density fluctuations of ordinary baryonic matter at the time of photon decoupling, the temperature anisotropies in the CMB would have to be at the level of 10^{-3} . However, the fact that they are actually two orders of magnitude smaller indicates that baryonic density perturbations can, in fact, not be the source of the required primordial wells of the gravitational potential. Instead these potential wells have to be attributed to some form of nonbaryonic dark matter that, unimpeded by photon pressure, is able to start clumping way before decoupling. Furthermore, numerical simulations of structure formation show that most dark matter has to be cold at the onset of structure formation, i.e. has to turn nonrelativistic long before the energy in matter begins to dominate over the energy in radiation.⁹

By now the overwhelming observational evidence has firmly established the notion that nonbaryonic cold dark matter (CDM) is the prevailing form of matter in the universe. It is thus one of the key ingredients to the Λ CDM model. Strong support for the CDM picture is again provided by the CMB power spectrum, which is next to the baryon density ρ_b also sensitive to the total matter density $\rho_m \propto \Omega_m h^2$ (cf. Sect. 2.2.1). Assuming dark matter to be cold and nonbaryonic, the combined CMB, BAO and H_0 data allow for a precise determination of $\Omega_m h^2$ [7],

$$\Omega_m^0 h^2 = 0.1349 \pm 0.0036, \quad (2.14)$$

which is roughly six times larger than the present baryon density $\Omega_b^0 h^2$ as inferred from the primordial abundances of the light elements or the CMB power spectrum. With the aid of Eqs. (2.12) and (2.14), the present density parameter of dark matter then turns out to be¹⁰

$$\Omega_{\text{DM}}^0 h^2 = \Omega_m^0 h^2 - \Omega_b^0 h^2 = 0.1123 \pm 0.0036, \quad \Omega_{\text{DM}}^0 \simeq 0.227. \quad (2.15)$$

⁸ The first astronomer to stumble upon the problem of the *missing mass* in galaxy clusters was Fritz Zwicky. In 1933, observations of the Coma Cluster led him to conclude that the galaxies in the cluster should actually fly apart, if there were not large amounts of invisible matter present in it, holding them together [41]. Zwicky is hence usually credited as the discoverer of dark matter.

⁹ As light neutrinos turn nonrelativistic only at very late times in the cosmological evolution, they represent, in fact, a form of hot dark matter in the current universe.

¹⁰ Later on we shall use a rounded version of the value in Eq. (2.15), namely $\Omega_{\text{DM}}^{\text{obs}} h^2 = 0.11$.

We thus know quite certainly that dark matter accounts for roughly 23 % of the energy budget of the universe. The nature and the origin of dark matter have, however, remained mysterious puzzles so far. At the present stage we are merely able to constrain to some extent its properties. First of all, the mismatch between determinations of $\Omega_b^0 h^2$ and $\Omega_m^0 h^2$, i.e. the present abundances of baryons in particular and of matter in general, as well as arguments based on the theory of structure formation indicate that dark matter has to be cold and nonbaryonic for the most part.¹¹ As it is *dark*, the particles constituting dark matter are usually assumed to be electrically neutral. Similarly, if these particles carried colour charge, they would strongly interact with baryons, thus altering, for instance, the predictions of BBN and the appearance of the CMB. Hence the dark matter particles are assumed to be colour-neutral. Finally, they have to be perfectly stable or at least sufficiently long-lived in order to explain the presence and influence of dark matter on cosmological time scales up to the current epoch. Interestingly, no known particle fulfills all these requirements and thus the existence of dark matter is one of the strongest indications for physics beyond the standard model. Particle cosmology now faces the task to identify which hypothetical new elementary particles could serve as dark matter particles, embed dark matter into a consistent picture of the cosmological evolution, and explain in particular how its present abundance is generated (cf. Eq. (2.15)). Therefore, the third key motivation of this thesis is to demonstrate that several well-motivated dark matter scenarios can actually be easily realized, if reheating after inflation is triggered by the B - L phase transition. For the most part, we will consider a scenario in which thermally produced gravitinos account for dark matter. In Chap. 8, we will then turn to a setup in which either higgsinos or winos represent the constituents of dark matter.

2.1.5 Dark Energy

A crucial result of our discussion so far is that dark matter, baryonic matter, neutrinos and photons together account for only roughly 27 % of the energy budget of the universe. The remaining 73 % have to be attributed to some form of dark energy that, as opposed to dark matter, does not cluster under the influence of gravity. At the present stage we almost do not know anything about the nature and the origin of dark energy, whereby dark energy represents one of the greatest mysteries of modern physics. At least some light on the properties of dark energy is shed by the fact that the expansion of our universe is currently accelerating.¹² As matter and radiation on their own always lead to either a decelerating expansion or an accelerated contraction, the

¹¹ Certain scenarios of warm dark matter or mixed dark matter which is composed of a mixture of cold, warm and or hot components, are also admissible [43, 44]. Likewise, also small amounts of baryonic matter in the form of massive compact halo objects (MACHOs) [45, 46] and or cold molecular gas clouds [47] may well contribute to the dark matter in galaxy halos.

¹² The accelerated expansion of our universe became evident for the first time in measurements of the distance-redshift relation of high-redshift type Ia SNe in 1998 [48, 49].

dark energy has to be responsible for the observed acceleration. Assuming that dark energy can be described as a perfect fluid, just as all other forms of matter and energy in the universe, the requirement that it be the source of the accelerated expansion constrains its equation of state, $\omega = p_{\text{DE}}/\rho_{\text{DE}} < -1/3$, where p_{DE} and ρ_{DE} denote the pressure and the energy density of dark energy, respectively. In other words: the accelerated expansion indicates that dark energy has a negative pressure.

There are several attempts to explain the presence of dark energy. Many approaches assume, for instance, that dark energy corresponds to the energy of a scalar field moving in some specific potential. Depending on whether this field has a canonical kinetic term or not, dark energy is then often referred to as quintessence [50, 51] or k essence [52]. An alternative possibility is that dark energy is entirely illusory, being in fact an artifact of an incorrect treatment of gravity. In this view, general relativity has to be modified in such a way that the accelerated expansion can be accounted for without any recourse to dark energy [53, 54]. The simplest solution, however, is provided by Einstein's cosmological constant Λ . Including a Λ term in the field equations of general relativity corresponds to adding a constant vacuum energy density $\rho_\Lambda = \Lambda/\kappa$ with $\kappa = 8\pi/M_p^2$ and equation of state $\omega = -1$ to the energy budget of the universe. Although this ansatz is the least sophisticated one, it is consistent with all observations and thus, along the lines of Occam's razor, the explanation of choice for dark energy in the Λ CDM model.¹³ Our earlier results for the density parameters of all other forms of matter and energy in the Λ CDM model then allow us to calculate the density parameter of dark energy [7],

$$\Omega_\Lambda^0 = \Omega_{\text{tot}}^0 - \Omega_{\text{DM}}^0 - \Omega_b^0 - \Omega_\nu^0 - \Omega_\gamma^0 = 0.728_{-0.016}^{+0.015}. \quad (2.16)$$

Finally, we remark that fitting the CMB, BAO and the SNe data from Ref. [10] to a relaxed version of the Λ CDM model, in which Ω_{tot} and ω are allowed to differ from 1 and -1 , respectively, yields a dark matter equation of state $\omega = -0.999_{-0.056}^{+0.057}$ [7], which is in excellent agreement with the assumption of a cosmological constant. For the moment being, as long as there is no commonly accepted explanation of dark energy in sight, we thus settle for a rather pragmatic approach and adopt the notion of a cosmological constant in this thesis, keeping in mind that it should be regarded as a placeholder for a future theory of dark energy that is still to come.

2.1.6 Stages in the Expansion History

The identification of the key items in the cosmic energy inventory as well as the determination of their respective contributions Ω_i^0 to the total energy density mark milestones of modern cosmology. Together with the current expansion rate H_0 , the

¹³ Naively one might expect the energy density of the vacuum to be related to the Planck scale, $\rho_\Lambda \sim M_p^4$. Interpreting dark energy as the energy of the vacuum, one then has to explain why $\rho_\Lambda \simeq 0.73\rho_c^0 \sim 10^{-123}M_p^4$. For a classic discussion of this so far unsolved problem cf. Ref. [55].

density parameters Ω_i^0 fully determine the present state of the universe on all scales on which the cosmological principle holds. On top of that, they also allow to trace the evolution of the universe back in time up to temperatures of $\mathcal{O}(1)$ MeV, i.e. until weak interactions begin to bring about interchanges between the abundances of the different species. Below the threshold for e^+e^- pair production, $T \ll m_e$, the energy densities of photons, matter and dark energy can, for instance, be written as functions of the cosmological redshift z in the following way,

$$T \ll m_e : \quad \rho_i(z) = \rho_c^0 \Omega_i^0 (1+z)^{3(1+\omega_i)}, \quad i = \gamma, m, \Lambda, \quad (2.17)$$

with ω_i denoting the coefficient in the equation of state of species i . We respectively have $\omega_\gamma = 1/3$, $\omega_m = 0$ and $\omega_\Lambda = -1$. The energy density of a nonrelativistic neutrino species with typical momentum p_{ν_i} and mass m_{ν_i} evolves similarly to the matter energy density ρ_m ,

$$p_{\nu_i}(z) \lesssim m_{\nu_i} : \quad \omega_{\nu_i} \approx 0, \quad \rho_{\nu_i}(z) \approx \frac{\rho_c^0}{h^2} \frac{m_{\nu_i}}{94 \text{ eV}} (1+z)^3. \quad (2.18)$$

Once the typical neutrino momenta p_{ν_i} begin to exceed m_{ν_i} , the respective neutrino species becomes relativistic,¹⁴ so that its energy density henceforth runs in parallel to ρ_γ ,

$$m_{\nu_i} \lesssim p_{\nu_i}(z) \ll m_e : \quad \omega_{\nu_i} \approx 1/3, \quad \rho_{\nu_i}(z) \approx \frac{7}{8} \left(\frac{4}{11} \right)^{4/3} \rho_\gamma(z). \quad (2.19)$$

The density of the total radiation energy is given as usual, $\rho_R(z) = g_{*,\rho}(z)/g_\gamma \rho_\gamma(z)$, with $g_{*,\rho}$ counting the effective number of relativistic degrees of freedom.

In the present epoch dark energy dominates the total energy of the universe, $\Omega_\Lambda^0 \gtrsim \Omega_m^0 \gg \Omega_\nu^0 \simeq \Omega_\gamma^0$. However, as the energy densities of radiation, matter and dark energy scale differently with redshift z , this changes as we go back in time. First, at $z = z_\Lambda$ the energy contained in matter catches up with dark energy, $\rho_m(z_\Lambda) = \rho_\Lambda(z_\Lambda)$. Then, at $z = z_{\text{eq}}$ radiation takes eventually over as the dominant form of energy in the universe, $\rho_R(z_{\text{eq}}) = \rho_m(z_{\text{eq}})$. The above scaling relations for the energy densities ρ_i imply

$$z_\Lambda = \left(\frac{\Omega_\Lambda^0}{\Omega_m^0} \right)^{1/3} - 1 \simeq 0.39, \quad z_{\text{eq}} = \frac{g_{*,\rho}^0 \Omega_m^0}{g_{*,\rho}^{\text{eq}} \Omega_\gamma^0} - 1 \simeq 3,200, \quad (2.20)$$

where we have used that $g_{*,\rho}^0 = 2$ and $g_{*,\rho}^{\text{eq}} = 2 + 7/8 \cdot 3 \cdot 2 \cdot (4/11)^{4/3} \simeq 3.36$. These two redshifts correspond to the following photon temperatures,

¹⁴ Given the allowed range of the total neutrino mass (cf. Eq. (2.7)), matching the two expressions for ρ_{ν_i} in Eqs. (2.18) and (2.19) and solving for z shows that the heaviest neutrino, which eventually contributes most to Ω_ν^0 , turns nonrelativistic at a redshift of $\mathcal{O}(10..100)$.

$$\begin{aligned} T_\Lambda &= T_\gamma(z_\Lambda) \simeq 3.8 \text{ K} \simeq 0.33 \text{ meV}, \\ T_{\text{eq}} &= T_\gamma(z_{\text{eq}}) \simeq 8,800 \text{ K} \simeq 0.76 \text{ eV}, \end{aligned} \quad (2.21)$$

as well as to the following values of the cosmic time t ,

$$t_\Lambda = t(z_\Lambda) \simeq 9.6 \text{ Gyr}, \quad t_{\text{eq}} = t(z_{\text{eq}}) \simeq 56 \text{ kyr}, \quad (2.22)$$

which are to be compared to the age of the universe, $t_0 = 13.75 \pm 0.13 \text{ Gyr}$ [7].

In summary, we conclude that the universe experiences at least three dynamically different stages in its expansion history. (i) In the very recent cosmic past, $z < z_\Lambda$, the energy of the universe is dominated by the vacuum contribution, which, due to its negative pressure, causes the expansion to accelerate. (ii) Between $z = z_\Lambda$ and $z = z_{\text{eq}}$ most energy is contained in pressureless matter. Note that it is in this epoch that matter structures are able to form in the universe.¹⁵ (iii) For $z > z_{\text{eq}}$ radiation is the most abundant form of energy in the universe. When speaking of the *hot thermal phase of the early universe* or the *hot early universe*, we actually refer to this phase of radiation domination. During the radiation-dominated era the universe is filled by a hot plasma in thermal equilibrium that becomes increasingly hotter and denser as one goes further back in time. In the approximation of a constant number of relativistic degrees of freedom $g_{*,\rho}$, the temperature $T \equiv T_\gamma$ of the thermal bath scales inversely proportional to $t^{1/2}$,

$$T(t) \approx \left(\frac{90M_P^2}{32\pi^3 g_{*,\rho} t^2} \right)^{1/4} \simeq 0.86 \text{ MeV} \left(\frac{43/4}{g_{*,\rho}} \right)^{1/4} \left(\frac{1 \text{ s}}{t} \right)^{1/2}, \quad (2.23)$$

where we have normalized $g_{*,\rho}$ to its value at the time of neutrino decoupling. As the temperature continues to rise, more and more particle species reach thermal equilibrium with the bath, causing $g_{*,\rho}$ to increase. Turning this picture around, we may equivalently say that in the hot early universe various species decouple one after another from the thermal bath in consequence of the declining temperature. These departures from thermal equilibrium shape the present state of the universe. Up to now we have already discussed the decoupling of neutrinos at $T \sim 1 \text{ MeV}$ and the decoupling of baryons at $T \sim 10 - 100 \text{ MeV}$. As we will see later on, similar nonequilibrium processes at even higher temperatures may be responsible for the relic density of dark matter and the baryon asymmetry of the universe. In fact, the very aim of this thesis is to describe a possible origin for the hot thermal phase of the early universe, namely the spontaneous breaking of $B-L$ at the end of inflation, that naturally entails the simultaneous generation of entropy, baryon asymmetry and dark matter.

¹⁵ Curiously enough, the matter-dominated era lasts sufficiently long to allow for the formation of such complex structures as galaxies, solar systems and human beings, which, from the perspective of mankind, appears to be a fortunate *cosmic coincidence*. The question of why dark energy becomes relevant exactly at the present time, i.e. why presently $\Omega_\Lambda \sim \Omega_m$ rather than $\Omega_\Lambda \ll \Omega_m$ or $\Omega_\Lambda \gg \Omega_m$, is one of the greatest puzzles of modern cosmology. Cf. e.g. Ref [56].

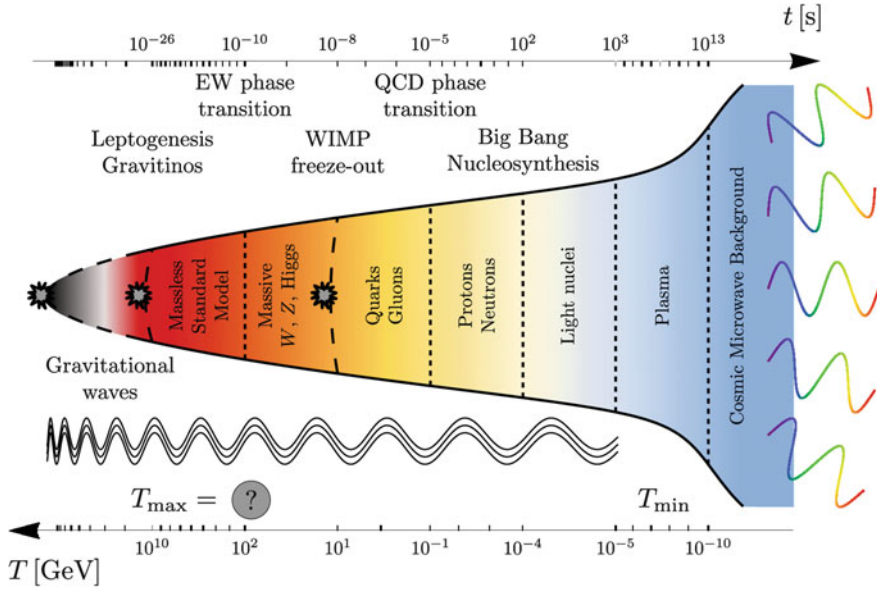


Fig. 2.1 Timeline of the hot thermal phase of the early universe illustrating (i) the relation between the temperature of the thermal bath T and the cosmic time t (cf. Eq. (2.23)), (ii) the chronology of several important, partly hypothetical nonequilibrium processes, (iii) a representative selection of those forms of matter or energy that are respectively involved in these processes, and (iv) several possibilities for the reheating temperature after inflation (cf. Sect. 3.1)

2.2 The Hot Thermal Phase

The hot early universe represents the stage for a great variety of physical processes taking place over an enormous range of energy scales (cf. Fig. 2.1 for an overview of the main events in its thermal history). As a final preparation before turning to our own scenario, we shall now discuss in more detail the decoupling of the CMB, primordial nucleosynthesis, the QCD and the electroweak phase transition as well as electroweak sphalerons.

2.2.1 The Cosmic Microwave Background

Towards the end of the radiation-dominated phase, at temperatures of $\mathcal{O}(1)$ eV, protons, i.e. hydrogen nuclei, are kept in thermal equilibrium via the steady interplay of radiative recombination and photoionization processes. However, as the plasma cools in the course of the expansion, photoionization becomes less efficient, the hydrogen nuclei begin to bind free electrons into neutral atoms and the ionization fraction of hydrogen freezes out at a vanishingly small value. This process is usually referred

to as hydrogen recombination.¹⁶ Due to the high abundance of thermal photons in the plasma it takes place at a temperature significantly below the binding energy of hydrogen, $B_H = 13.6$ eV. In fact, the temperature has to drop to $T_{\text{rec}} \simeq 0.30$ eV until the fractional ionization reaches a value of 10 %. As the abundance of free electrons continues to decrease even further, the rate Γ_γ of Thomson scatterings between thermal photons and plasma electrons falls below the Hubble rate H . At $T_{\text{dec}} \simeq 0.26$ eV the mean free photon path equals the Hubble radius H^{-1} , or equivalently $\Gamma_\gamma = H$, and most photons scatter for the last time. This moment of *last scattering* marks the time when the photons decouple and the universe becomes transparent to radiation. After decoupling the photons freely propagate until they eventually reach us in the form of CMB radiation. In this sense the CMB represents a full-sky picture of the early universe at a temperature of $T_{\text{dec}} \simeq 0.26$ eV, i.e. at a redshift $z_{\text{dec}} \simeq 1,100$ and a cosmic time $t_{\text{dec}} \simeq 360$ kyr.

To be precise, the decoupling of the CMB actually occurs during the matter-dominated era (cf. T_{eq} in Eq. (2.21)). But as its origin is inextricably linked with the thermal history of the universe, it represents nonetheless one of the main physical phenomena associated with the hot big bang [57]. In particular, the fact that the CMB has an almost perfect Planckian spectrum may be regarded as key evidence for an early stage during which the universe was filled by a hot plasma in thermal equilibrium. Alternative attempts to explain the origin of the CMB, such as the idea put forward by the proponents of the steady state theory proposing that the CMB may in fact be starlight thermalized by dust grains, typically end up with a superposition of blackbody spectra corresponding to different temperatures.

The CMB not only provides striking evidence for the hot thermal phase, as we have seen in Sect. 2.1, it also allows to precisely determine a multitude of cosmological parameters that enter into the theoretical description of the early universe.¹⁷ The primary CMB observable encoding cosmological information is the variation of the CMB temperature across the sky, which is conveniently characterized by the angular power spectrum C_ℓ of the relative temperature fluctuations,

$$\frac{\delta T}{T_0}(\mathbf{n}) = \sum_{\ell=2}^{\infty} \sum_{m=-\ell}^{+\ell} a_{\ell m} Y_{\ell m}(\mathbf{n}) , \quad \langle a_{\ell m}^* a_{\ell' m'} \rangle = C_\ell \delta_{\ell\ell'} \delta_{mm'} . \quad (2.24)$$

Except for the dipole anisotropy, which is interpreted as being due to the motion of the earth relative to the absolute CMB rest frame, the CMB temperature anisotropies directly correspond to the density perturbations inherent in the baryon-photon fluid at the time of last scattering. Several physical processes leave their imprint in the observed power spectrum. (i) The tight coupling between photons and baryons leads to higher temperatures in regions of high baryon density. (ii) Photons that have to

¹⁶ Prior to hydrogen recombination, at $T \sim 0.5$ eV, helium decouples in a similar way. As hydrogen is still fully ionized at this time, the universe remains opaque after helium recombination.

¹⁷ For reviews on the physics of the CMB and its potential to constrain cosmological models, cf. for instance Refs. [58, 59].

climb out of potential wells after decoupling are gravitationally redshifted. This translates into a shift of the observed with respect to the intrinsic temperature fluctuation, which is usually referred to as the Sachs-Wolfe effect [60]. Similarly, decaying gravitational potentials traversed by the CMB photons on their way from the surface of last scattering to the observer induce small boosts in the observed CMB temperature. This is known as the integrated Sachs-Wolfe effect. (iii) The non-zero velocity of the plasma at decoupling results in a Doppler shift in the frequency of the CMB photons. (iv) Perturbations in the gravitational potential, induced by the growing density fluctuations of dark matter, as well as photon pressure drive acoustic oscillations in the photon-baryon fluid, which gives rise to a series of acoustic peaks in the CMB power spectrum.¹⁸ These four effects, but in particular the acoustic peaks, are very sensitive to the parameters of the underlying cosmology. Barring a few degeneracies, the CMB power spectrum encodes information about at least ten basic cosmological parameters.

First of all, four parameters characterize the power spectra of primordial density fluctuations as well as primordial gravitational waves. These primordial scalar and tensor perturbations, as they are also referred to, eventually evolve into the CMB temperature fluctuations. The parameters characterizing their power spectra, P_s and P_t , hence determine the initial conditions for the evolution of the CMB anisotropies. Usually, P_s and P_t are taken to be power-laws,

$$P_s(k) = A_s \left(\frac{k}{k_*} \right)^{n_s-1}, \quad P_t(k) = A_t \left(\frac{k}{k_*} \right)^{n_t}, \quad r = \frac{A_t}{A_s}, \quad (2.25)$$

where k is the comoving momentum scale and k_* stands for an arbitrary reference scale. Technically, P_s denotes the power spectrum of the curvature perturbation \mathcal{R} , which measures the spatial curvature of a comoving slicing of spacetime. P_t represents in fact the sum of two power spectra, P_+ and P_\times , which respectively account for the two physical polarization modes h_+ and h_\times of the general traceless and transverse spatial metric perturbation. Note that due to rotational invariance $P_+ = P_\times = P_t/2$. The great virtue of the three perturbations \mathcal{R} , h_+ and h_\times is that they are time-independent at early times, i.e. as long as they extend over scales larger than the Hubble radius H^{-1} . So far, the CMB data has revealed no sign of tensor modes. Thus, only the curvature perturbation amplitude A_s as well as the scalar spectral index n_s have been measured up to now. Neglecting potential tensor contributions and using a reference scale $k_* = 0.002 \text{ Mpc}^{-1}$, the combined WMAP, BAO and H_0 data yields [7],

$$A_s = \left(2.441_{-0.092}^{+0.088} \right) \times 10^{-9}, \quad n_s = 0.963 \pm 0.012, \quad (2.26)$$

¹⁸ Perturbations in the photon-baryon fluid can only evolve causally as long as they extend over scales smaller than the sound horizon. This explains the position of the first acoustic peak in the CMB power spectrum. It is located at an angular scale of roughly 1° or equivalently at $\ell \sim 200$, which corresponds to the angular diameter of the sound horizon at last scattering.

For comparison, the COBE data implies an amplitude $A_s \simeq 2.28 \times 10^{-9}$ at roughly the same scale k_* . This result is usually referred to as the COBE normalization of the scalar power spectrum [61]. WMAP, BAO and the SNe data from Ref. [10] together yield a tight upper bound on the tensor-to-scalar ratio, $r < 0.20$ at 95 % CL. A measurement of the tensor spectral index n_t is beyond the scope of any experiment in the near future. In single-field slow-roll models of inflation (cf. Sect. 3.1) n_t does not represent an independent parameter in any case. It is rather directly related to the tensor-to-scalar ratio via the *consistency relation*, $n_t = -r/8$, which reduces the number of free parameters fixing the initial conditions of the CMB anisotropies to three. The background cosmology setting the stage for the evolution of the CMB anisotropies is described by at least five parameters: the expansion rate H_0 , the energy densities of matter and baryons, or equivalently $\Omega_m^0 h^2$ and $\Omega_b^0 h^2$, the density parameter of dark energy Ω_{DE}^0 , and the coefficient ω in the equation of state for dark energy. In Sect. 2.1, we discussed in detail the numerical values of these parameters according to the CMB data in combination with other cosmological observations. Finally, one astrophysical parameter influences the CMB power spectrum: the integrated optical depth τ , which characterizes the amount of CMB photons that undergo Thomson scattering owing to the reionization of the universe in the recent cosmic past. τ completes the set of standard parameters usually included in analyses of the CMB power spectrum. Beyond this set further parameters, such as the density of massive neutrinos $\Omega_\nu^0 h^2$ or the running of the scalar spectral index $dn_s/d \ln k$, may be taken into account as well.

While the CMB stands out as one of the main pillars of the picture of the big bang, it also shows very plainly some of the severe problems big bang cosmology is facing with regard to its initial conditions. First of all, the observation that presently Ω_{tot} does not deviate by more than 1 % from unity gives rise to the *flatness problem*. In a decelerating universe the deviation from exact flatness always grows as some power of the cosmic time.¹⁹ The total density parameter Ω_{tot} of a universe exhibiting a small, but non-zero curvature in the present epoch must hence approach unity to arbitrary precision as one goes back in time. In other words, the initial value of Ω_{tot} must be unnaturally fine-tuned. Second, at the time of last scattering the past or particle horizon, i.e. the distance scale characterizing the radial extent of causally connected domains, is of $\mathcal{O}(100)$ Mpc corresponding to an angular diameter of $\mathcal{O}(1^\circ)$ in the sky. By contrast, the CMB is highly isotropic across the entire sky, which is to say that at the time of decoupling the photon temperature is almost perfectly homogeneous over a huge number of causally disconnected regions. Again, this high degree of homogeneity can only be achieved by an unnatural fine-tuning of the initial conditions, a puzzle which is known as the *horizon problem*. Furthermore, the minute deviations from an exactly isotropic temperature, that we do observe in the CMB, finally lead to the third and perhaps most severe problem. The mechanism responsible for the high degree of homogeneity over a multitude of causally disconnected regions also has to

¹⁹ Given a scale factor $a \propto t^p$, $\Omega_{tot} - 1$ scales like $\dot{a}^{-2} \propto t^{2(1-p)}$. During the phases of radiation and matter domination we respectively have $p = 1/2$ and $p = 2/3$.

explain why the temperature fluctuations around the homogeneous background are precisely at the level of 10^{-5} and, in particular, why they are correlated over scales exceeding the causal horizon at decoupling. This problem may be translated into the following two fundamental questions: (i) what is the origin of the primordial scalar and tensor perturbations and (ii) which statistical properties do they have? As we will see in Sect. 3.1, all these three problems concerning the initial conditions of the hot big bang can be successfully solved in inflationary cosmology.

2.2.2 Primordial Nucleosynthesis

Primordial or big bang nucleosynthesis (BBN), i.e. the generation of the light elements during the first 20 min of the radiation-dominated era, represents the earliest testable nonequilibrium process in the history of the universe which can be accounted for by well-understood standard model physics only (cf. Fig. 2.1).²⁰ At present it hence provides the deepest reliable probe of the early universe. The overall agreement of the observed primordial abundances of the light elements with the predictions of BBN serves as a strong corroboration of hot big bang cosmology, underpinning our picture of the early universe to a similar extent as the anisotropies in the CMB.

Before the onset of BBN, at temperatures $T \gg 1$ MeV or correspondingly at times $t \ll 1$ s, the weak interactions $n \nu_e \rightleftharpoons p e^-$, $n e^+ \rightleftharpoons p \bar{\nu}_e$, and $n \rightleftharpoons p e^- \bar{\nu}_e$ keep the neutron-to-proton ratio n/p in thermal equilibrium, $n/p = e^{-Q/T}$ with $Q = m_n - m_p = 1.293$ MeV denoting the neutron-proton mass difference. Around a temperature of 1 MeV the rate of neutron-proton interconversion processes Γ_{np} eventually drops below the Hubble rate H and the neutron-to-proton ratio freezes out at $n/p \simeq 1/6$. Subsequent to freeze-out, n/p still continues to decrease due to neutrons undergoing β^- decay, $n \rightarrow p e^- \bar{\nu}_e$. At the time the neutrons decouple from the thermal bath, the temperature has already fallen below the binding energy of deuterium, $T \sim 1$ MeV $< \Delta_D \simeq 2.23$ MeV. The synthesis of deuterium, however, does not yet commence because of the large abundance of highly energetic photons that immediately dissociate each newly formed deuterium nucleus. This delay in the production of the light elements is referred to as the *deuterium bottleneck*. It is overcome once the number of photons per baryon above the deuterium photodissociation threshold has decreased below unity, which happens at a temperature $T \sim 0.1$ MeV or roughly at the end of the first three minutes. The breaking of the deuterium bottleneck marks the onset of BBN. At last deuterium can be efficiently produced and further processed into heavier elements such as helium-3, helium-4 and lithium-7.

Independently of the nuclear reaction rates, virtually all free neutrons end up bound in helium-4, which is the most stable one among the light elements. At $T \sim 0.1$ MeV the neutron-to-proton ratio has decreased to $n/p \simeq 1/7$ and the primordial mass fraction of helium-4 can be estimated as

²⁰ For reviews on BBN, cf. for instance Refs. [62, 63].

$$Y_p = \frac{4 n_{\text{He}}}{n_b} \approx \frac{4 (n_n/2)}{n_p + n_n} = \frac{2 n/p}{1 + n/p} \simeq 25 \%, \quad (2.27)$$

which corresponds to a ratio by number of helium-4 to hydrogen of ${}^4\text{He}/\text{H} \simeq 8\%$. Deuterium, helium-3 and lithium-7 are produced in much smaller numbers. At the end of BBN around $t \sim 20$ min, when the temperature has dropped to $T \sim 0.03$ MeV and most nuclear reactions have become inefficient, D/H and ${}^3\text{He}/\text{H}$ are of $\mathcal{O}(10^{-5})$, while ${}^7\text{Li}/\text{H}$ is of $\mathcal{O}(10^{-10})$. The complicated network of nuclear reactions that lead to these primordial abundances is described by a coupled system of kinetic equations that needs to be solved numerically [64, 65]. Besides the temperature T or equivalently the cosmic time t , the Hubble rate and the nuclear reaction rates that enter into these equations are functions of only one cosmological parameter: the number density of baryons n_b during BBN. As n_b is directly related to the present value of the BAU, $n_b = n_\gamma g_{*,s}/g_{*,s}^0 \eta_B^0$, this explains why the observed primordial abundances of the light elements give us a handle on η_B^0 (cf. Sect. 2.1.3).

The abundance of primordial deuterium is inferred from spectra of high-redshift quasar absorption systems, while primordial helium-4 is observed in low-metallicity regions of ionized hydrogen. The spectra of old metal-poor, i.e. population II stars in the spheroid of our galaxy allow to determine the primordial abundance of lithium-7. All in all, the theoretical BBN predictions match the observed abundances of deuterium, helium-4 and lithium-7 quite well within the η_B^0 range stated in Eq. (2.11).²¹ An obvious curiosity, however, is that the lithium-7 abundance points to a value of η_B^0 that is smaller by at least 4.2σ than the value jointly favoured by the abundances of deuterium and helium-4. This discrepancy is known as the *lithium problem* [66] and potentially indicates effects of new physics.

Leaving aside the lithium problem, we conclude that BBN is able to correctly predict the primordial abundances of the light elements over a range of nine orders magnitude. This success is a milestone of big bang cosmology, encouraging us to believe that the laws of physics which we are able to test in laboratory experiments also apply to the very first moments of the universe. We are thus confident that modern particle physics allows us to speculate about the history of the universe at still earlier times, $t \ll 1$ s, although as of now we have no means of observationally accessing them. Furthermore, the success of BBN provides us with a powerful tool to constrain deviations from the standard cosmology.

The helium-4 abundance, for instance, is very sensitive to the value of $g_{*,\rho}$ and thus the presence of additional relativistic species during BBN [67]. Increasing $g_{*,\rho}$ above its standard value entails a faster Hubble expansion, which results in the neutrons decoupling at earlier times. The neutron-to-proton ratio then freezes out at a correspondingly higher temperature, leading to a larger abundance of primordial helium-4 (cf. Eq. (2.27)). Deviations from the standard value of $g_{*,\rho}$ are usually

²¹ Data on helium-3 solely derives from the solar system and high-metallicity regions of ionized hydrogen in our galaxy, which makes it difficult to infer its primordial abundance. On top of that, the theory of stellar helium-3 synthesis is in conflict with observations. For these two reasons, helium-3 is usually not used as a cosmological probe.

parametrized in terms of an effective number of neutrino species $N_{\text{eff}} = N_{\text{eff}}^{\text{st}} + \Delta N_{\text{eff}}$. Before e^+e^- annihilation, $N_{\text{eff}}^{\text{st}}$ is given as $N_{\text{eff}}^{\text{st}} = 3.046$ [68] and $g_{*,\rho}$ is related to N_{eff} through $g_{*,\rho} = 2 + 7/8 \cdot (4 + N_{\text{eff}} \cdot 2)$. It turns out that the primordial helium-4 mass fraction scales with ΔN_{eff} as $\Delta Y_p \simeq 0.013 \Delta N_{\text{eff}}$ [69], which allows to place limits on N_{eff} by means of the measured abundance of primordial helium-4. In combination with the seven-year WMAP data, one finds $N_{\text{eff}} < 4.2$ at 95 % CL [70].

Likewise, the late-time decay of a massive nonrelativistic particle which is not included in the standard BBN scenario may as well alter the primordial abundances of the light elements. Similarly to additional relativistic species, the presence of such a particle modifies the expansion rate prior to its decay. On top of that, if the new particle dominates the energy density of the universe at the time of its decay, a significant amount of entropy is produced while its decay products thermalize. This changes the time-temperature relationship and results in a diluted baryon-to-photon ratio. Based on these effects, one can derive an upper bound on the lifetime of the decaying particle or equivalently a lower bound on the temperature of the thermal bath at the time the entropy production is completed [71]. If the process of entropy production shortly before BBN is identified with the reheating of the universe after inflation, this lower bound on the temperature corresponds to the lowest possible value of the reheating temperature $T_{\text{RH}}^{\text{min}}$ (cf. Sect. 3.1.1). Combining the observed primordial abundances of deuterium and helium-4 with CMB and LSS data, one obtains $T_{\text{RH}}^{\text{min}} \simeq 4 \text{ MeV}$ at 95 % CL [72].

Independently of whether a long-lived massive particle dominates the energy density of the universe or not, it may after all spoil the success of standard BBN through the cascade processes induced by its decay. Charged particles or photons emitted in radiative decays of the long-lived particle entail electromagnetic showers [73]. Sufficiently energetic photons produced in these showers are then able to photodisintegrate previously formed light nuclei. Moreover, given appropriate couplings and on condition that they are kinematically allowed, decays into colour-charged particles trigger hadronic cascade processes [74]. These involve energetic pions, kaons, neutrons, protons as well as the corresponding antiparticles, all of which are able to react with the light nuclei in various ways. The hadrons emitted in the decays of the long-lived particle induce, for instance, extraordinary interconversion processes between the background nucleons. This leads to an enhancement of the neutron-to-proton ratio after neutron decoupling and thus to a larger abundance of helium-4. At the same time, the energetic hadrons are also able to dissociate background helium-4 nuclei and to produce the other light elements nonthermally. If the decaying particle is electrically charged, it can form bound states with background nuclei, which again changes the nuclear reaction rates. Especially, the production of lithium-6 may be catalyzed in this way [75].

In order to determine the net effect of a long-lived massive particle on the primordial abundances of the light elements, it is necessary to compute the distributions of the various decay products of the decaying particle as functions of time. These spectra then allow to calculate the rates of the photo- and hadrodissociation, neutron-proton interconversion, and nonstandard production processes induced by the decay of the unstable particle. Requiring the impact of the decaying particle to remain

small, such that the consistency between the theoretical BBN predictions and the astrophysical observations is maintained, one can derive constraints on the mass, lifetime and abundance of the unstable particle prior to its decay [76, 77]. In Chap. 8 we will in particular consider bounds on the properties of a very heavy gravitino decaying shortly before BBN [78].

2.2.3 Phase and Topological Transitions

The synthesis of the light elements marks the earliest process in the hot early universe that is firmly established on the basis of observations.²² The exact nature of all nonequilibrium processes occurring prior to BBN, such as the generation of the BAU or the primordial metric perturbations, are currently still subject to speculations. On the other hand, the standard model of particle physics describes the interactions of elementary particles with great precision all the way up to the TeV scale. Based on standard model physics one is thus able to make an educated guess about the history of the universe up to $T \sim 1$ TeV or equivalently $t \sim 10^{-13}$ s. In the following we shall in particular elaborate on the phase and topological transitions which presumably take place in the very early universe.

QCD Phase Transition

At temperatures well above the scale of quantum chromodynamics (QCD),²³ $T \gg \Lambda_{\text{QCD}} \simeq 220$ MeV, most quarks, antiquarks and gluons interact only very weakly with each other. Instead of being bound in baryons or mesons, they freely propagate through the thermal bath as independent degrees of freedom, forming what is referred to as a quark-gluon plasma. However, as the temperature decreases, the strong force becomes increasingly stronger, until at a temperature $T \sim 100$ MeV all colour-charged particles get confined in hadrons, i.e. pions for the most part. This transition from the quark-gluon plasma to hadronic matter is known as the QCD or quark-gluon phase transition (cf. Fig. 2.1). Its order parameter, ξ_{QCD} , keeping track of the progress of the QCD transition as it unfolds, is given by the vacuum expectation value (VEV) of the quark condensate operator, $\xi_{\text{QCD}} = \langle \bar{q}_L q_R + \bar{q}_R q_L \rangle$. While ξ_{QCD} initially vanishes, it is of $\mathcal{O}(\Lambda_{\text{QCD}}^3)$ at the end of the QCD phase transition. As the quark condensate operator transforms nontrivially under chiral transformations, we conclude that the QCD phase transition entails the spontaneous breaking of the global chiral symmetry in the quark sector. We also note that, according to numerical lattice calculations, the QCD phase transition is most likely a smooth crossover rather than

²² Recall that BBN enables us to trace the evolution of the hot thermal phase up to temperatures as high as $T_{\text{RH}}^{\text{min}} \simeq 4$ MeV or equivalently cosmic times as early as $t \simeq 0.05$ s (cf. Sect. 2.2.2).

²³ The QCD scale Λ_{QCD} corresponds to the energy scale at which, according to its renormalization group running in perturbative QCD, the strong coupling constant g_s formally diverges.

a first or second order phase transition. One thus expects that it does not leave any observationally detectable imprint in the cosmic evolution.

Electroweak Phase Transition

The QCD phase transition is believed to be preceded by the electroweak (EW) phase transition, occurring close to the Fermi or electroweak scale $v_{EW} \simeq 174 \text{ GeV}$ (cf. Fig. 2.1). At temperatures $T \gg v_{EW}$ all standard model particles are massless and the universe is said to be in the symmetric phase. The order parameter of the electroweak phase transition, ξ_{EW} , is identified with the VEV of the Higgs product operator $H^\dagger H$, with H denoting the standard model Higgs doublet, $\xi_{EW} = \langle H^\dagger H \rangle$. By definition, ξ_{EW} vanishes in the symmetric phase. Once the temperature drops below a critical value T_{EW} , the Higgs boson $h \in H$, the electroweak gauge bosons and all fermions except for neutrinos acquire masses through the Higgs mechanism. This is reflected in the order parameter ξ_{EW} obtaining a nonzero value that approaches v_{EW}^2 in the zero-temperature limit. Both the explicit value of T_{EW} as well as the order of the electroweak phase transition depend on the Higgs boson mass m_h . The LHC experiments ATLAS and CMS recently presented hints that the Higgs boson may have a relatively large mass, $m_h \simeq 125 \text{ GeV}$ [79, 80]. Based on this value for m_h , one finds $T_{EW} \simeq 170 \text{ GeV}$ [3]. Furthermore, given $m_h \simeq 125 \text{ GeV}$, the electroweak phase transition turns out to be a smooth crossover without any dramatic cosmological consequences.

After the phase transition the universe is in the Higgs phase and the electroweak symmetry is said to be spontaneously broken to the electromagnetic symmetry,

$$SU(2)_W \times U(1)_Y \rightarrow U(1)_{EM}. \quad (2.28)$$

This terminology is, however, not quite correct as $H^\dagger H$ transforms as a singlet under all gauge transformations, so that the electroweak symmetry remains intact even after the electroweak phase transition. What happens instead is a rearrangement of the physical degrees of freedom, proceeding in such a way that after the phase transition the electroweak symmetry is realized in a nonlinear fashion. It would hence be more appropriate to speak of the electroweak symmetry as being *hidden* subsequent to the phase transition. However, as it is more common to refer to it as being *broken*, we will adopt this terminology in the following.²⁴ We note that this discussion applies in particular also to the B – L phase transition, during which the B – L gauge symmetry actually becomes hidden rather than broken.

²⁴ Likewise, when referring to some Higgs product operator $s^\dagger s$ acquiring a VEV v , we will also sometimes write $v = \langle s \rangle$, although we actually mean $v = \langle s^\dagger s \rangle^{1/2}$.

Electroweak Instanton and Sphaleron Transitions

As the temperature approaches the electroweak scale, also nonperturbative processes which simultaneously violate baryon number B and lepton number L gain in importance. Their emergence is a direct consequence of the fact that the electroweak dynamics are governed by a chiral and non-Abelian gauge theory. First of all, we note that both global $U(1)_B$ and $U(1)_L$ transformations represent accidental symmetries of the standard model Lagrangian. Hence, both B and L are conserved in the standard model at the classical level. Due to the chiral nature of the electroweak interactions, they are, however, violated at the quantum level through the triangle anomaly, which results in the divergences of the baryon and lepton number currents, J_B^μ and J_L^μ , being nonzero [81, 82],

$$\partial_\mu J_B^\mu = \partial_\mu J_L^\mu = \frac{N_f}{32\pi^2} \varepsilon^{\mu\nu\sigma\tau} \left(-g_W^2 \text{Tr } W_{\mu\nu} W_{\sigma\tau} + g_Y^2 B_{\mu\nu} B_{\sigma\tau} \right). \quad (2.29)$$

Here, N_f counts the number of fermion families, $\varepsilon^{\mu\nu\sigma\tau}$ represents the Levi-Civita symbol in four dimensions, $W_{\mu\nu}^a$ and $B_{\mu\nu}$ are the field strength tensors of the weak and hypercharge gauge fields, and g_W and g_Y denote the corresponding gauge couplings. The second ingredient to the nonconservation of B and L is the complicated structure of the vacuum of the $SU(2)_W$ gauge theory. As for any non-Abelian gauge theory, the $SU(2)_W$ vacuum manifests itself in infinitely many, homotopically distinct,²⁵ pure gauge configurations, each of which is characterized by a specific integer topological charge or Chern-Simons number N_{CS} . An important observation is that distinct realizations of the $SU(2)_W$ vacuum differing by $\Delta N_{\text{CS}} = 1$ are connected to each other via a non-contractible loop in field configuration space [83]. The field configuration of highest energy along this path is known as the sphaleron [84]. Corresponding to a saddle-point of the energy functional of the gauge-Higgs system, the sphaleron represents a classical, spatially localized and static, but unstable solution of the electroweak field equations. Its energy E_{sph} determines the height of the potential barrier by which two adjacent realizations of the $SU(2)_W$ vacuum are separated,

$$E_{\text{sph}}(T) \simeq \frac{8\pi}{g_W} \sqrt{2} v_{\text{EW}}(T), \quad v_{\text{EW}}(T) = \xi_{\text{EW}}^{1/2}(T). \quad (2.30)$$

Now combining the nontrivial topology of the $SU(2)_W$ vacuum with the fact that the currents J_B^μ and J_L^μ have nonzero divergences (cf. Eq. (2.29)), one can show that both B and L are violated in topological vacuum transitions,

$$\Delta B = \Delta L = N_f \Delta N_{\text{CS}}. \quad (2.31)$$

In the standard model, in which we have $N_f = 3$, the smallest jump in B and L is hence $\Delta B = \Delta L = \pm 3$. The difference between B and L is, by contrast,

²⁵ Gauge configurations belonging to different homotopy classes are transformed into each other via *large* gauge transformations.

always conserved in topological transitions. This is also evident from the vanishing divergence of the B - L current, $\partial_\mu J_{B-L}^\mu = \partial_\mu J_B^\mu - \partial_\mu J_L^\mu = 0$ (cf. Eq. (2.29)).

Topological transitions between different realizations of the $SU(2)_W$ vacuum come in two different varieties. One possibility is tunneling *through* the potential barrier via $SU(2)_W$ instantons. The instanton rate is, however, proportional to $\exp(-16\pi^2/g_W^2) \sim 10^{-170}$ and thus severely suppressed. This is to say that in the standard model B - and L -violating processes are completely negligible at low temperature. On the other hand, in the hot plasma filling the universe during the radiation-dominated era, thermal fluctuations can lead to sphaleron transitions *over* the potential barrier [85]. In the Higgs phase, the sphaleron rate is proportional to $\exp(-E_{\text{sph}}/T)$ [86] and hence becomes unsuppressed as soon as $T \gtrsim E_{\text{sph}}$. Although the barrier is large at zero temperature, $E_{\text{sph}} \simeq 10 \text{ TeV}$, it rapidly melts away as the temperature approaches the critical value T_{EW} from below (cf. Eq. (2.30)). That is why sphalerons already reach thermal equilibrium at a temperature slightly below the critical temperature, $T_{\text{sph}}^{\text{min}} \sim T_{\text{EW}} - 10 \text{ GeV}$ [87], rather than at temperatures as high as 10 TeV . Conversely, we may say that at $T_{\text{sph}}^{\text{min}}$ the sphaleron processes freeze-out, so that for $T \ll T_{\text{sph}}^{\text{min}}$ both B and L are conserved. This means in particular that at the latest around $T = T_{\text{sph}}^{\text{min}}$ the baryon asymmetry is fixed to its present value.

During the restoration of the electroweak symmetry the potential barrier vanishes completely. Hence, the actual sphaleron configuration in the sense of a saddle-point of the energy functional no longer exists in the symmetric phase. Instead, at $T > T_{\text{EW}}$, topological transitions occur due to thermal fluctuations in the electroweak gauge fields. In the following we shall, however, refer to these transitions as sphaleron processes nonetheless. In the symmetric phase, sphaleron transitions occur at rate per unit volume $\Gamma_{\text{sph}}/V \propto \alpha_W^5 T^4$ [88] where $\alpha_W = g_W^2/(4\pi)$. This result can be used to show that sphalerons are in thermal equilibrium up to a temperature $T_{\text{sph}}^{\text{max}} \sim 10^{12} \text{ GeV}$. At higher temperatures the sphaleron rate is again outweighed by the expansion rate.

Above the electroweak scale all standard model gauge and Yukawa interactions as well as the electroweak sphaleron and QCD instanton processes are in thermal equilibrium. This implies relations between the chemical potentials of all fermions and Higgs particles, which, together with the requirement that the total hypercharge of the thermal bath be zero, can be used to derive the sphaleron-driven equilibrium values of B and L [89],

$$B = C_{\text{sph}}(B-L), \quad L = (C_{\text{sph}} - 1)(B-L), \quad C_{\text{sph}} = \frac{8N_f + 4N_H}{22N_f + 13N_H}, \quad (2.32)$$

with N_H denoting the number of Higgs doublets. The standard model (SM) only contains one Higgs doublet H , while in its minimal supersymmetric extension, the minimal supersymmetric standard model (MSSM), two Higgs doublets, H_u and H_d , are required in order to ensure anomaly freedom,

$$\text{SM: } N_H = 1, C_{\text{sph}} = \frac{28}{79} \quad \text{MSSM: } N_H = 2, C_{\text{sph}} = \frac{8}{23}. \quad (2.33)$$

From Eq.(2.32) we conclude that if $B-L = 0$, sphaleron processes always completely wash out any baryon asymmetry, which is generated in some nonequilibrium process at $T \gg T_{\text{sph}}^{\min}$. By contrast, as $B-L$ is conserved in topological transitions, any primordial $B-L$ asymmetry is guaranteed to survive until sphaleron freeze-out. From this perspective, the baryon asymmetry, which we presently observe in the universe, points to a nonequilibrium process above the electroweak scale that is responsible for the generation of a primordial $B-L$ asymmetry. As we will see in Sect. 3.1.3, leptogenesis is a prime candidate for such a process. Let us denote the time when the $B-L$ -violating process, i.e. leptogenesis in our case, terminates by t_f . The present value of the baryon asymmetry or baryon-to-photon ratio η_B is then related to the primordial $B-L$ in the following way,

$$\eta_B^0 = \left. \frac{n_B}{n_\gamma} \right|_{t_0} = C_{\text{sph}} \left. \frac{n_{B-L}}{n_\gamma} \right|_{t_0} = C_{\text{sph}} \frac{g_{*,s}^0}{g_{*,s}} \left. \frac{n_{B-L}}{n_\gamma} \right|_{t_f}. \quad (2.34)$$

References

1. E.W. Kolb, M.S. Turner, The early universe. *Front. Phys.* **69**, 1–547 (1990)
2. S. Dodelson, *Modern Cosmology* (Academic University Press, Amsterdam, 2003)
3. V. Mukhanov, *Physical foundations of cosmology* (University Press, Cambridge, UK, 2005)
4. M. Trodden, S. M. Carroll, TASI lectures: Introduction to cosmology. [astro-ph/0401547]
5. V. Rubakov, *Introduction to Cosmology*, PoS(RTN2005)003 (2005)
6. K. Nakamura et al. (Particle Data Group), Review of particle physics, *J. Phys.G* **G37**, 075021 (2010)
7. E. Komatsu et al. (WMAP Collaboration), Seven-year WMAP observations: cosmological interpretation, *Astrophys. J.Suppl.* **192**, 18 (2011)
8. W.J. Percival et al., (SDSS Collaboration), Baryon acoustic oscillations in the sloan digital sky survey data release 7 galaxy sample. *Mon. Not. Roy. Astron. Soc.* **401**, 2148–2168 (2010)
9. A.G. Riess, L. Macri, S. Casertano, M. Sosey, H. Lampeitl et al., A redetermination of the hubble constant with the hubble space telescope from a differential distance ladder. *Astrophys. J.* **699**, 539–563 (2009). [0905.0695]
10. M. Hicken, W. Wood-Vasey, S. Blondin, P. Challis, S. Jha et al., Improved dark energy constraints from 100 new CfA supernova type ia light curves. *Astrophys. J.* **700**, 1097–1140 (2009). [0901.4804]
11. R. Kessler, A. Becker, D. Cinabro, J. Vanderplas, J. A. Frieman et al. First-year sloan digital sky survey-II (SDSS-II) supernova results: hubble diagram and cosmological parameters, *Astrophys. J.Suppl.* **185**, 32–84 (2009). [0908.4274]
12. M. Kowalski et al., (Supernova Cosmology Project), Improved cosmological constraints from new, old and combined supernova datasets. *Astrophys. J.* **686**, 749–778 (2008). [0804.4142]
13. J.C. Mather, E. Cheng, D. Cottingham, R. Eplee, D. Fixsen et al., Measurement of the cosmic microwave background spectrum by the coBE FIRAS instrument. *Astrophys. J.* **420**, 439–444 (1994)
14. J.C. Mather, D. Fixsen, R. Shafer, C. Mosier, D. Wilkinson, Calibrator design for the COBE far infrared absolute spectrophotometer (FIRAS). *Astrophys. J.* **512**, 511–520 (1999). [astro-ph/9810373]

15. G.F. Smoot, C. Bennett, A. Kogut, E. Wright, J. Aymon et al., Structure in the COBE differential microwave radiometer first year maps. *Astrophys. J.* **396**, L1–L5 (1992)
16. D. Fixsen, The temperature of the cosmic microwave background. *Astrophys. J.* **707**, 916–920 (2009). [0911.1955]
17. M. Archidiacono, E. Calabrese, A. Melchiorri, The case for rark radiation. *Phys. Rev.* **D84**, 123008 (2011). [1109.2767]
18. C.A. Egan, C.H. Lineweaver, A larger estimate of the entropy of the universe. *Astrophys. J.* **710**, 1825–1834 (2010). [0909.3983]
19. A. Ringwald, Prospects for the direct detection of the cosmic neutrino background. *Nucl. Phys.* **A827**, 501C–506C (2009). [0901.1529]
20. S. Hannestad, Primordial neutrinos. *Ann. Rev. Nucl. Part. Sci.* **56**, 137–161 (2006). [hep-ph/0602058]
21. T.L. Smith, S. Das, O. Zahn, Constraints on neutrino and dark radiation interactions using cosmological observations. *Phys. Rev.* **D85**, 023001 (2012)
22. S. Fukuda et al., (Super-Kamiokande Collaboration), Tau neutrinos favored over sterile neutrinos in atmospheric muon-neutrino oscillations. *Phys. Rev. Lett.* **85**, 3999–4003 (2000). [hep-ex/0009001]
23. Q. Ahmad et al., (SNO Collaboration), Measurement of the rate of $\nu_e + d \rightarrow p + p + e^-$ interactions produced by ^8B solar neutrinos at the Sudbury Neutrino Observatory. *Phys. Rev. Lett.* **87**, 071301 (2001). [nucl-ex/0106015]
24. W. Hu, D.J. Eisenstein, M. Tegmark, Weighing neutrinos with galaxy surveys. *Phys. Rev. Lett.* **80**, 5255–5258 (1998). [astro-ph/9712057]
25. J. Lesgourgues, S. Pastor, Massive neutrinos and cosmology. *Phys. Rept.* **429**, 307–379 (2006). [astro-ph/0603494]
26. S.A. Thomas, F.B. Abdalla, O. Lahav, Upper bound of 0.28 eV on the neutrino masses from the largest photometric redshift survey. *Phys. Rev. Lett.* **105**, 031301 (2010). [0911.5291]
27. M. Fukugita, P.E. Peebles, The cosmic energy inventory. *Astrophys. J.* **616**, 643–668 (2004). [astro-ph/0406095]
28. R. Cen, J.P. Ostriker, Where are the baryons? *Astrophys. J.* **514**, 1 (1999). [astro-ph/9806281]
29. W. Buchmuller, R. Peccei, T. Yanagida, Leptogenesis as the origin of matter. *Ann. Rev. Nucl. Part. Sci.* **55**, 311–355 (2005). [hep-ph/0502169]
30. G. Steigman, When clusters collide: constraints on antimatter on the largest scales. *J. Cosmol. Astropart. Phys.* **0810**, 001 (2008). [0808.1122]
31. A.G. Cohen, A. De Rujula, S. Glashow, A matter-antimatter universe? *Astrophys. J.* **495**, 539–549 (1998). [astro-ph/9707087]
32. G. Bertone, D. Hooper, J. Silk, Particle dark matter: evidence, candidates and constraints. *Phys. Rept.* **405**, 279–390 (2005). [hep-ph/0404175]
33. J. Einasto, Dark Matter. [0901.0632]
34. D. Hooper, TASI 2008 Lectures on Dark Matter. [0901.4090]
35. G. Bertone (ed.), *Particle Dark Matter: Observations, Models and Searches* (Cambridge University Press, Cambridge, 2010), p. 738
36. M. Milgrom, A modification of the newtonian dynamics as a possible alternative to the hidden mass hypothesis. *Astrophys. J.* **270**, 365–370 (1983)
37. J.D. Bekenstein, Relativistic gravitation theory for the MOND paradigm. *Phys. Rev.* **D70**, 083509 (2004). [astro-ph/0403694]
38. V.C. Rubin, J. Ford, W. Kent, Rotation of the andromeda nebula from a spectroscopic survey of emission regions. *Astrophys. J.* **159**, 379–403 (1970)
39. S. Faber, R. Jackson, Velocity dispersions and mass to light ratios for elliptical galaxies. *Astrophys. J.* **204**, 668 (1976)
40. R. Catena, P. Ullio, A novel determination of the local dark matter density. *J. Cosmol. Astropart. Phys.* **1008**, 004 (2010). [0907.0018]
41. F. Zwicky, Die rotverschiebung von extragalaktischen nebeln. *Helv. Phys. Acta* **6**, 110–127 (1933)

42. D. Clowe, M. Bradac, A.H. Gonzalez, M. Markevitch, S.W. Randall et al., A direct empirical proof of the existence of dark matter. *Astrophys. J.* **648**, L109–L113 (2006). [astro-ph/0608407]
43. M. Viel, J. Lesgourgues, M.G. Haehnelt, S. Matarrese, A. Riotto, Constraining warm dark matter candidates including sterile neutrinos and light gravitinos with WMAP and the Lyman-alpha forest. *Phys. Rev.* **D71**, 063534 (2005). [astro-ph/0501562]
44. K. Jedamzik, M. Lemoine, G. Moulta, Gravitino, axino Kaluza-Klein graviton warm and mixed dark matter and reionisation. *J. Cosmol. Astropart. Phys.* **0607**, 010 (2006). [astro-ph/0508141]
45. B. Paczynski, Gravitational microlensing by the galactic halo. *Astrophys. J.* **304**, 1–5 (1986)
46. P. Tisserand et al., (EROS-2 Collaboration), Limits on the macho content of the galactic halo from the eros-2 survey of the magellanic clouds. *Astron. Astrophys.* **469**, 387–404 (2007). [astro-ph/0607207]
47. F. De Paolis, G. Ingrosso, P. Jetzer, M. Roncadelli, A case for a baryonic dark halo. *Phys. Rev. Lett.* **74**, 14–17 (1995). [astro-ph/9410016]
48. A.G. Riess et al., (Supernova Search Team), Observational evidence from supernovae for an accelerating universe and a cosmological constant. *Astron. J.* **116**, 1009–1038 (1998). [astro-ph/9805201]
49. S. Perlmutter et al., (Supernova Cosmology Project), Measurements of Omega and Lambda from 42 high redshift supernovae. *Astrophys. J.* **517**, 565–586 (1999). [astro-ph/9812133], The Supernova Cosmology Project
50. B. Ratra, P. Peebles, Cosmological consequences of a rolling homogeneous scalar field. *Phys. Rev.* **D37**, 3406 (1988)
51. C. Wetterich, Cosmology and the fate of dilatation symmetry. *Nucl. Phys.* **B302**, 668 (1988)
52. C. Armendariz-Picon, V.F. Mukhanov, P.J. Steinhardt, Essentials of k essence. *Phys. Rev.* **D63**, 103510 (2001). [astro-ph/0006373]
53. B. Jain, P. Zhang, Observational tests of modified gravity. *Phys. Rev.* **D78**, 063503 (2008). [0709.2375]
54. T. Clifton, P.G. Ferreira, A. Padilla, C. Skordis, Modified gravity and cosmology. *Phys. Rept.* **513**, 1–189 (2012)
55. S. Weinberg, The cosmological constant problem. *Rev. Mod. Phys.* **61**, 1–23 (1989)
56. I. Zlatev, L.-M. Wang, P.J. Steinhardt, Quintessence, cosmic coincidence, and the cosmological constant. *Phys. Rev. Lett.* **82**, 896–899 (1999). [astro-ph/9807002]
57. R. Dicke, P. Peebles, P. Roll, D. Wilkinson, Cosmic black-body radiation. *Astrophys. J.* **142**, 414–419 (1965)
58. W. Hu, S. Dodelson, Cosmic microwave background anisotropies. *Annu. Rev. Astron. Astrophys.* **40**, 171–216 (2002). [astro-ph/0110414]
59. D. Samtleben, S. Staggs, B. Winstein, The cosmic microwave background for pedestrians: a review for particle and nuclear physicists. *Annu. Rev. Nucl. Part. Sci.* **57**, 245–283 (2007). [0803.0834]
60. R. Sachs, A. Wolfe, Perturbations of a cosmological model and angular variations of the microwave background. *Astrophys. J.* **147**, 73–90 (1967)
61. E.F. Bunn, A.R. Liddle, M. White, Four year COBE normalization of inflationary cosmologies. *Phys. Rev.* **D54**, 5917–5921 (1996). [astro-ph/9607038]
62. K.A. Olive, G. Steigman, T.P. Walker, Primordial nucleosynthesis: theory and observations. *Phys. Rep.* **333**, 389–407 (2000). [astro-ph/9905320]
63. F. Iocco, G. Mangano, G. Miele, O. Pisanti, P.D. Serpico, Primordial Nucleosynthesis: from precision cosmology to fundamental physics. *Phys. Rep.* **472**, 1–76 (2009)
64. R.V. Wagoner, W.A. Fowler, F. Hoyle, On the synthesis of elements at very high temperatures. *Astrophys. J.* **148**, 3–49 (1967)
65. R.H. Cyburt, B.D. Fields, K.A. Olive, The NACRE thermonuclear reaction compilation and big bang nucleosynthesis. *New Astron.* **6**, 215–238 (2001). [astro-ph/0102179]
66. R.H. Cyburt, B.D. Fields, K.A. Olive, An Update on the big bang nucleosynthesis prediction for Li-7: The problem worsens. *J. Cosmol. Astropart. Phys.* **0811**, 012 (2008). [0808.2818]

67. G. Steigman, D. Schramm, J. Gunn, Cosmological limits to the number of massive leptons. *Phys. Lett.* **B66**, 202–204 (1977)
68. G. Mangano, G. Miele, S. Pastor, T. Pinto, O. Pisanti et al., Relic neutrino decoupling including flavor oscillations. *Nucl. Phys.* **B729**, 221–234 (2005). [hep-ph/0506164]
69. J. Bernstein, L.S. Brown, G. Feinberg, Cosmological helium production simplified. *Rev. Mod. Phys.* **61**, 25 (1989)
70. G. Mangano, P.D. Serpico, A robust upper limit on N_{eff} from BBN, circa. *Phys. Lett.* **B701**, 296–299 (2011). [1103.1261]
71. M. Kawasaki, K. Kohri, N. Sugiyama, Cosmological constraints on late time entropy production. *Phys. Rev. Lett.* **82**, 4168 (1999). [astro-ph/9811437]
72. S. Hannestad, What is the lowest possible reheating temperature? *Phys. Rev.* **D70**, 043506 (2004). [astro-ph/0403291]
73. R.H. Cyburt, J.R. Ellis, B.D. Fields, K.A. Olive, Updated nucleosynthesis constraints on unstable relic particles. *Phys. Rev.* **D67**, 103521 (2003). [astro-ph/0211258]
74. M. Kawasaki, K. Kohri, T. Moroi, Hadronic decay of late-decaying particles and Big-Bang nucleosynthesis. *Phys. Lett.* **B625**, 7–12 (2005). [astro-ph/0402490]
75. M. Pospelov, Particle physics catalysis of thermal big bang nucleosynthesis. *Phys. Rev. Lett.* **98**, 231301 (2007). [hep-ph/0605215]
76. M. Kawasaki, K. Kohri, T. Moroi, Big bang nucleosynthesis and hadronic decay of long-lived massive particles. *Phys. Rev.* **D71**, 083502 (2005). [astro-ph/0408426]
77. K. Jedamzik, Big bang nucleosynthesis constraints on hadronically and electromagnetically decaying relic neutral particles. *Phys. Rev.* **D74**, 103509 (2006). [hep-ph/0604251]
78. M. Kawasaki, K. Kohri, T. Moroi, A. Yotsuyanagi, Big bang nucleosynthesis and gravitino. *Phys. Rev.* **D78**, 065011 (2008)
79. G. Aad et al., (ATLAS Collaboration), Combined search for the standard model higgs boson using up to 4.9 fb^{-1} of pp collision data at $\sqrt{s} = 7 \text{ TeV}$ with the ATLAS detector at the LHC. *Phys. Lett.* **B710**, 49–66 (2012). [hep-ph/9809381]
80. S. Chatrchyan et al., (CMS), Combined results of searches for the standard model higgs boson in pp collisions at $\sqrt{s} = 7 \text{ TeV}$. *Phys. Lett.* **B710**, 26–48 (2012). [1202.1408]
81. G. 't Hooft, Symmetry breaking through bell-jackiw anomalies. *Phys. Rev. Lett.* **37**, 8–11 (1976)
82. G. 't Hooft, Computation of the quantum effects due to a four-dimensional pseudoparticle. *Phys. Rev.* **D14**, 3432–3450 (1976)
83. N. Manton, Topology in the Weinberg-Salam Theory. *Phys. Rev.* **D28**, 2019 (1983)
84. F.R. Klinkhamer, N. Manton, A saddle Point solution in the Weinberg-Salam theory. *Phys. Rev.* **D30**, 2212 (1984)
85. V. Kuzmin, V. Rubakov, M. Shaposhnikov, On the anomalous electroweak baryon number nonconservation in the early universe. *Phys. Lett.* **B155**, 36 (1985)
86. P.B. Arnold, L.D. McLerran, Sphalerons, small fluctuations and baryon number violation in electroweak theory. *Phys. Rev.* **D36**, 581 (1987)
87. H. Klapdor-Kleingrothaus, S. Kolb, V. Kuzmin, Light lepton number violating sneutrinos and the baryon number of the universe. *Phys. Rev.* **D62**, 035014 (2000). [hep-ph/9909546]
88. P.B. Arnold, L.G. Yaffe, Nonperturbative dynamics of hot non-abelian gauge fields: beyond leading log approximation. *Phys. Rev.* **D62**, 125013 (2000). [hep-ph/9912305]
89. S.Y. Khlebnikov, M. Shaposhnikov, The statistical theory of anomalous fermion number non-conservation. *Nucl. Phys.* **B308**, 885–912 (1988)

The B–L Phase Transition

Implications for Cosmology and Neutrinos

Schmitz, K.

2014, XIII, 221 p. 19 illus., 10 illus. in color., Hardcover

ISBN: 978-3-319-00962-9